Manuscript ID: 1361
DOI: 10.18462/iir.icr.2019.1361

Development of a dynamic model for ice-on-coil external melt storage systems

Jasper NONNEMAN[a,b], Michiel DE VOS[a], Hugo MONTEYNE[a], Wim BEYNE[a], Michel DE PAEPE[a,b]

[a] Department of Flow, Heat and Combustion Mechanics, Ghent University, Sint-Pietersnieuwstraat 41, 9000 Ghent, Belgium, Jasper.Nonneman@UGent.be
[b] Flanders Make, Core Lab MotionS, Gaston Geenslaan 8, 3001, Leuven, Belgium

ABSTRACT

Ice storage systems are commonly used to balance the intermittency of renewable energy and decrease the peak load by switching to off-peak hours. An adequate model is necessary to predict the behaviour of these systems. However, there is a scarce in detailed models available used to describe the performance of an ice storage evaporator and its use in a refrigeration cycle. Most existing models approximate the working principles with a steady analysis, not considering the sub cooling of ice and thickness distribution along the length. The developed model in this article uses a discretisation in length and radial direction together with an adapted thermal resistance matrix method to limit the calculation time. It has a great variability of boundary conditions and the ability to implement different types of refrigerants. The simulation results are in good agreement with the data of the manufacturer. The model shows that switching from R404A to R449A reduces the total electricity consumption.
Keywords: Cold Storage, Evaporator, Ice Bank, Modelling, R404A, R449A

1. INTRODUCTION

Present day, renewable power generation is quickly growing all over the world. Questions arise about their intermittent generation and as a result the continuous need of backup systems which are more polluting (Steinke et al., 2013). Moreover, the boost of air conditioning systems with a growth from 1.6 billion today to an expected 5.6 billion by 2050 requires a new electricity capacity equivalent to the combined electricity capacity of US, EU and Japan today. Together with this, air conditioning systems are also responsible for a major part of the peak loads, especially during the summer and/or in hot climates (Goetzler et al., 2016). During these peak moments, less efficient and more polluting peak plants are required. To balance both the demand and the intermittent generation of renewable energy methods, a storage method can be used to introduce both a spatial as well as a temporal dissociation between production and usage. This paper focuses on the use of a cool thermal storage. The charging during off-peak hours or when there is a surplus of renewable energy has the possibility to drastically reduce the peak load and consequently electricity costs by switching parts from on- to off-peak hours (Cárdenas & León, 2013; Saito, 2002).
Different cool thermal storage options exist, but the focus in this paper is on ice thermal storage which benefits from the large value of the latent heat of fusion compared to the sensible heat. In a narrow temperature range, a high volumetric capacity can be reached with these systems (Biosca-Taronger et al., 2012). An ice-on-coil external melt system will be discussed in this work, which is charged by a refrigerant flowing inside the coils and discharged by water flowing over the ice coils (see Figure 1). Consequently, no ice bridging between the different coils is allowed to ensure the circulation of the water over the ice coils during discharging. Ice is formed outside of the coils and due to the increased thickness of the ice, the thermal resistance of the ice rises and as a result, the effectiveness decreases. This is a characteristic of a static thermal energy storage; the ice is built and stored at the same location and no complex harvesting techniques are required in contrast to a dynamic thermal energy storage (Saito, 2002).

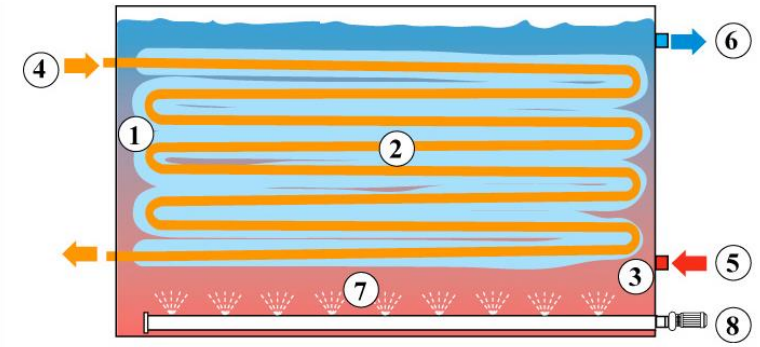

Figure 1: Ice-on-coil external melt working principle (Baltimore, 2019)

With a constant evaporator temperature, the ice thickness increases non-linearly with a decreasing slope due to the increased thermal resistance with ice thickness. Consequently, the evaporating temperature has to be decreased to ensure the uniform continuation of the ice formation when connected to a condensing unit. Due to the decrease in evaporating temperature, the cooling power delivered by the condensing unit/refrigerant decreases as well. Most numerical models approach the working principle of the ice storage as a perfect heat transfer of two flows. The ice formation is obtained by $Q_{ice} = \Delta T_f \dot{m}_f c_{p,f}$ in the case of a single phase coolant, with Q_{ice} the cooling capacity, ΔT_f the difference between the inlet and outlet temperature of the charge flow, $\dot{m}_f$ the mass flow rate of the charge flow and $c_{p,f}$ the specific heat capacity of the charge flow (Vetterli & Benz, 2012). Moreover, environmental conditions and consequently losses to the environment are not taken into account in most models found in scientific literature. To take into account the increase of ice resistance and therefore the decrease in effectiveness, an effectiveness curve ε in function of the fraction of ice is implemented in the majority of the models. This curve is obtained from experimental data and is added to the equation for the cooling power: $Q_{ice} = \varepsilon \Delta T_f \dot{m}_f c_{p,f}$. This equation is used both for the charging and the discharging process with a different slope (Candanedo et al., 2013). This gives an idea about the cooling power, but no further insights in the working principle or possible adaptations/optimisations can be obtained from these models.
Furthermore, a switch from R404A to R449A is recently proposed in the refrigeration systems due to its lower global warming potential which is almost three times smaller. As with R404A, no chlorine is present in R449A and consequently, the ozone depletion potential is zero. Little research has been done, but the results are promising: similar energy performances are obtained after the switch. The major drawback is found in the temperature glide of 5.8 °C at 0.1 MPa for R449A which is only 0.8 °C at the same pressure for R404A (Makhnatch et al., 2017; Tecumseh, 2016). Because of the lack of adequate models to predict the performance of ice-on-coil external melt storage systems, a dynamic model is developed in this work, with a great variability of boundary conditions and the ability to implement different types of refrigerants. With this model, the two refrigerants R404A to R449A will be investigated.

2. DYNAMIC NUMERICAL MODEL

The numerical model is based on the thermal resistance matrix method for one phase materials/fluids, although adapted to account for phase changes. The different nodes *i* are thermally connected to each other and as a result, this method is based on the discretized energy balances between the nodes. The node temperatures are obtained in the regular thermal resistance matrix method by $T=K^{-1}b$ with K the conductance matrix, T the array of node temperatures and b the array of heat inputs:

$$K_{ij} = K_{ji} = R_{ij}^{-1} = R_{ji}^{-1} \quad \text{Eq. (1)}$$

$$K_{ii} = -(\Sigma_{j \neq i} K_{ij} + \Sigma R_{ext,i}^{-1} + m_i c_{p,i} \Delta t^{-1}) \quad \text{Eq. (2)}$$

$$b_i = -(Q_i + \Sigma T_{ext,i} R_{ext,i}^{-1} + m_i c_{p,i} \Delta t^{-1} T_{i,t-1}) \quad \text{Eq. (3)}$$

Where R is the thermal resistance, i and j represent the different nodes, m_i the mass in node i, Δt the discretised time step and *ext* refers to external nodes. When a phase change occurs, the temperature stays constant and only the enthalpy changes. As a result, the previously defined equations can no longer be used for this node. The array of node temperatures T is changed to an array of node temperatures and/or enthalpies TH where TH_k is the enthalpy in node k; the node where ice is formed or melted. The other elements still represent the corresponding node

temperature. Consequently, column k in the K matrix that interacts with TH_i has to be adapted. A characteristic of node k with an enthalpy in the range $[-H_{lat};0]$ is that the temperature is equal to the melting temperature until the enthalpy exceeds the limits of the range defined. An enthalpy of zero is considered for water at melting temperature and an enthalpy of $-H_{lat}$ corresponds to ice at melting temperature. The regular resistance matrix method can be used with the following additions to account for the change from temperature to enthalpy for one node:

$$K_{kk} = -m_k \, \Delta t^{-1} \quad \text{Eq. (4)}$$

$$K_{k\pm1,k} = 0 \quad \text{Eq. (5)}$$

$$b_k = \Sigma_{i\neq k} K_{ki} \, T_{melt} + \Sigma \, T_{melt} \, R_{ext,k}^{-1} - (Q_k + \Sigma \, T_{ext,k} \, R_{ext,k}^{-1} + m_k \, \Delta t^{-1} H_{k,t-1}) \quad \text{Eq. (6)}$$

$$b_{k\pm1} = -K_{k,k\pm1} \, T_{melt} - (Q_{k\pm1} + \Sigma \, T_{ext,k\pm1} \, R_{ext,k\pm1}^{-1} + m_{k\pm1} \, c_{p,k\pm1} \, \Delta t^{-1} T_{k\pm1,t-1}) \quad \text{Eq. (7)}$$

The energy balances are based only on sensible heat for layers with only ice or only water. A layer which is partially filled with ice is based on the latent heat and consequently, the enthalpy difference with a known temperature and state.

A division into different layers and in sections of length is proposed in this model. The outer radius of the last layer is defined by the maximum radius the ice can reach to ensure no ice bridging. Due to the division into different layers, a thermal capacitance per layer is taken into account and every time step the total ice layers are calculated to update the ice resistances. This division in sections of length is introduced to take into account the effect of the temperature glide of the refrigerant which is not negligible for R449A, and consequently resulting in a different ice thickness over the length of the coil. The energy balances obtained from this division into different layers are visualized by the thermal equivalent circuit shown in Figure 2 for an example with two full ice layers and a division into four equivalent layers.

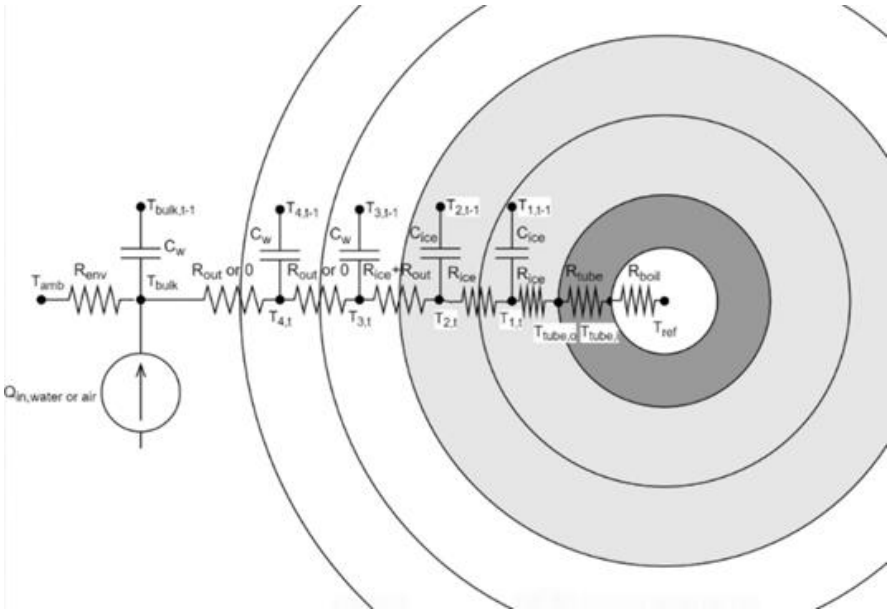

Figure 2: Thermal equivalent circuit for two full ice layers.

The heat transfer of the refrigerant at the inside of the coil which is a two-phase flow, is calculated with the Shah correlation (Shah, 1976) for heat transfer during boiling flow through pipes (Lee & Jones, 1996). This correlation is based on the consideration that the nucleate boiling and the convective boiling are the two most important heat transfer mechanisms where the larger one is chosen as the value to approach the local two-phase boiling heat transfer coefficient. The heat transfer at the outside of the coil is dependent on the mass flow rate of the water or in general when charging or discharging occurs. In case of a mass flow of water (during discharging), forced convection correlations are used which are based on the Reynolds number, $Re=v \, \rho \, (2r) \, \mu^{-1}$, with v the fluid velocity, ρ the density, r the ice radius and μ the fluid viscosity. During charging, there is no incoming mass flow rate of water, so natural convection occurs and this is based on the Rayleigh number Ra. The Rayleigh number (a dimensionless number defining whether heat in a fluid is transferred primarily by free convection or conduction) is expressed by $Ra=(2r)^3 g\beta(T_{wall} - T_\infty) \, \rho^2 c_p \mu^{-1}$

with β the thermal expansion coefficient, T_{wall} the outer temperature of the (ice) coil and T_{∞} the average tank temperature. The density curve of water has its maximum point around 4 °C so further cooling down shows a negative thermal expansion coefficient and a switch of the stratification of the water inside the tank.
Convection correlations from scientific literature are compared which are able to handle this sign difference and the correlation of Merk is chosen in the model. This correlation is based on a cylinder in a tank with a certain bulk water temperature similar to an ice storage tank and experimental results found in literature showed a small deviation for a large range of conditions (Yen, 1990). This correlation only describes the heat transfer from bulk fluid temperature to the tube wall, but does not provide a temperature distribution of the fluid around the coil. The flow characteristic per layer and consequently the temperature in the middle of this water layer is approached by a division of the outer resistance equally between every node. As a result, a temperature gradient is obtained between the bulk temperature and the water layer temperature closest to the coil. For the discharging process, on the other hand, the whole tank is assumed to be perfectly mixed due to the circulating water and no temperature gradient is present close to the coil. With this approach, every node has the same temperature as the tank temperature on that height level. The ambient conditions are taken into account by the calculation of the losses to the environment. At the outside this is based on natural convection of the air. Dependent on the mass flow rate of water, forced or natural convection correlations are used at the inside of the wall.
During the discharging, water is circulated through the tank with a certain mass flow rate and to facilitate this discharging process, air is introduced from an air blower. This air is released at the bottom of the tank through pipes with a small perforation. Two sources of heat inputs (incoming water and air flow) are present and are taken into account, but only the water flow is taken into account to calculate the forced convection resistance. Nevertheless, air will promote the heat transfer, so an enhancement factor can be estimated based on experiments to reduce the deviations between the simulations and the experiments.

3. SIMULATION RESULTS

3.1. Evaporator model

The described model is further used to simulate a 1.28 m high, 1.15 m wide and 1.8 m long ice storage tank with five evaporator coils of 13.85 m long and with an outer diameter of 6.25 mm. The coils are made of copper and are positioned such that the maximum ice radius on a coil before ice bridging is 38 mm. The simulations are done for only one coil, so the total length of the tank (1.8 m) is divided by 5. In this part (evaporator model), a constant refrigerant inlet temperature and mass flow rate are assumed. Both a charging cycle and discharging cycle are investigated.

3.1.1. Charging cycle

First, the charging of the ice tank is evaluated with the refrigerant R449A at 270 K inlet temperature and a mass flow rate of 0.0084 kgs^{-1}, which is equally distributed over the 5 coils. The water in the tank is initially at 278 K and the ambient temperature is 293.15 K. The simulations are done with a time step of 180 s and the total charging time is 5 h. In Figure 3 and Figure 4 a comparison is shown between the total ice capacity after 5 h of charging and the amount of respectively layer or section divisions that were used in the simulation. The temperature glide has been neglected if the length is not divided into different sections. As a result, this case is an overestimation of the cooling capacity. This error drops quite fast and from the moment the length is divided into 15 sections the relative error is below 1 % compared to the defined limit value of 40 which is visualized in Figure 3.
A small amount of different layers is expected to be an overestimation of the system because the temperatures taken are only an average over the entire layer, which introduces an error on the ice formation. With a division into layers, a relative error of less than 0.2 % is reached with a division into 25 layers compared to the defined limit value of 60 divisions. The defined limit values are visualized in the graphs by the dashed line (Figure 4). The evaporator model for charging is further validated by the evaluation of the equality of the energy balances. The cooling power supplied by the refrigerant should be equal to the energy used to cool the ice/water and the losses to the environment. The difference does not exceed 0.2 W in absolute terms, which is a consequence of the iterations that are done to converge the model.

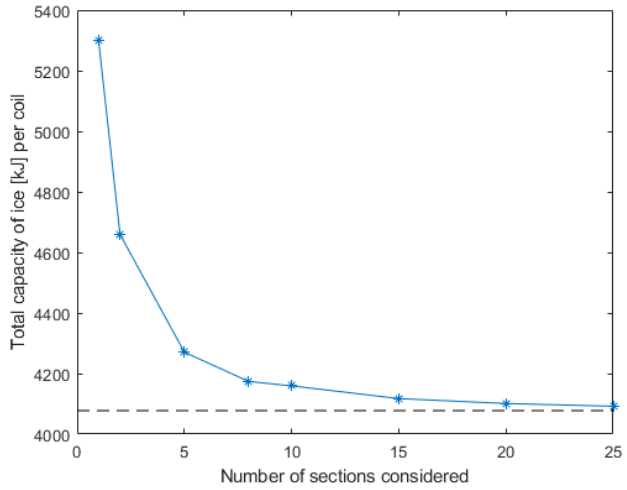

Figure 3: Influence of the total amount of section divisions on the total capacity of ice per coil after 5 hours of charging.

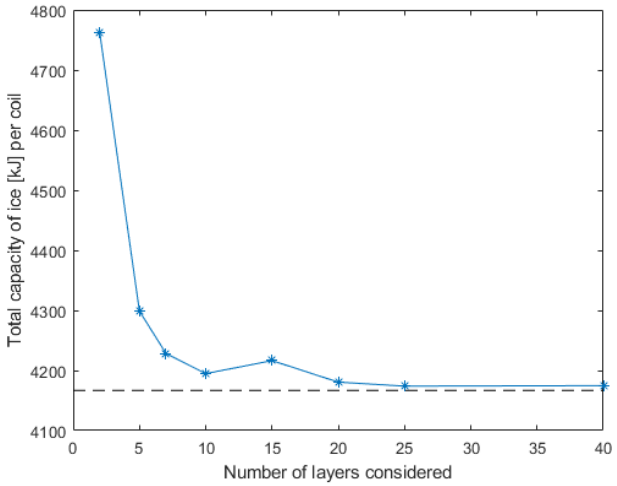

Figure 4: Influence of the division into different layers on the total mass of ice after 5 hours charging.

3.1.2. Discharging cycle

The discharging time is evaluated to validate the time span of discharging which should be in the range of 30 to 60 min according to the manufacturer. At the start of the discharging, the tank and content are at a temperature of 273.65 K and with a 55.4 kg initial mass of ice. The mass flow rate of the hot water entering the tank is 1.933 kgs^{-1} and is assumed to be divided equally over the 5 coils. With a varying inlet temperature of the water, the mass of ice per coil is visualized within time in Figure 5. In Figure 6 the effectiveness curve in function of the fraction of ice of the discharge simulation is compared to one from Henze and Krarti (Ihm et al., 2004), and they show a similar trend. Next to these validations, the energy balances are compared to ensure no energy is lost. No iterations occur here, because the forced convection correlation is independent of unknown temperatures in contrast to the charging process. As a result, the absolute error is at its maximum $12x10^{-5}$ W.

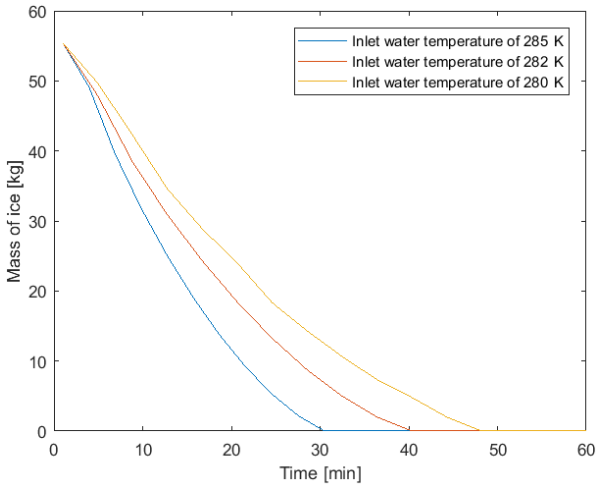

Figure 5: Mass of ice during a discharging process with a varying inlet water temperature.

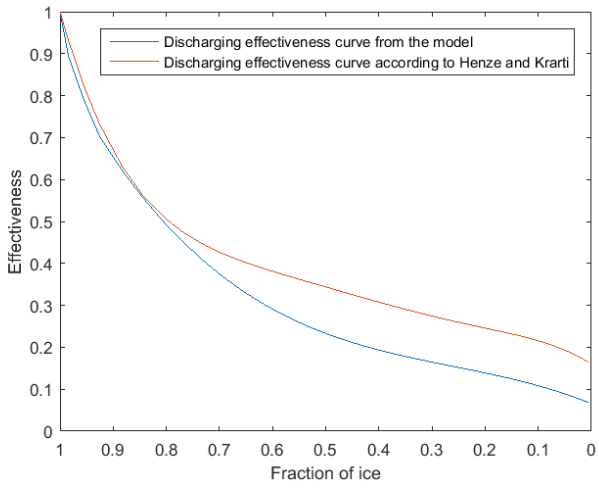

Figure 6: Effectiveness curve in function of the fraction of ice obtained from the model and according to Henze and Krarti. (Ihm et al., 2004)

3.2. Evaporator model coupled to condensing unit

Next the evaporator model is coupled to a condensing unit. Based on data of the condensing unit TFHT4531ZHR from Tecumseh (Tecumseh, 2016), polynomials are obtained by data fitting for the cooling power and mass flow rate of the refrigerant. The model is connected to these data and iterated till the cooling power in the model is equal to the cooling power delivered by the condensing unit. The cooling power delivered by the refrigerant drops after time due to the increased thermal

resistance of ice. To ensure the ice formation, the evaporating temperature and mass flow rate of the refrigerant decreases as well. With initially no ice in the tank and an initial temperature of 273.65 K, a charging time of 5.9 h is achieved.

3.2.1. Comparison R404A and R449A

Recently, a switch from R404A to R449A in air conditioning systems is proposed. A lower GWP and ODP are the reasons for this switch but little research has been done on the effect on the performances of this switch. Based on simulations of a charging cycle with both refrigerants, they can be compared under the same conditions and with the same condensing unit. The differences in performance after a charging cycle of 5.9 h are shown in Table 1 for the two refrigerants. The total mass and capacity of ice is larger with the use of R404A, which can be explained by the more even distribution of the ice thickness along the length. This can be seen in Figure 7 where the thickness distribution along the length is shown. The more even distribution results in a higher total mass of ice when one point reaches the maximum radius. Furthermore, the opposite sign of the slopes is clearly noticed. This phenomenon is explained by the combination of a different temperature glide and the convection coefficient by boiling along the length.

Table 1: Performance comparison after a complete charging cycle.

Parameter	Theoretical maximum	R449A	R404A
Ice mass [kg]	*55.4*	*51.1*	*52.8*
Ice capacity [MJ]	*18.5*	*17.3*	*17.9*

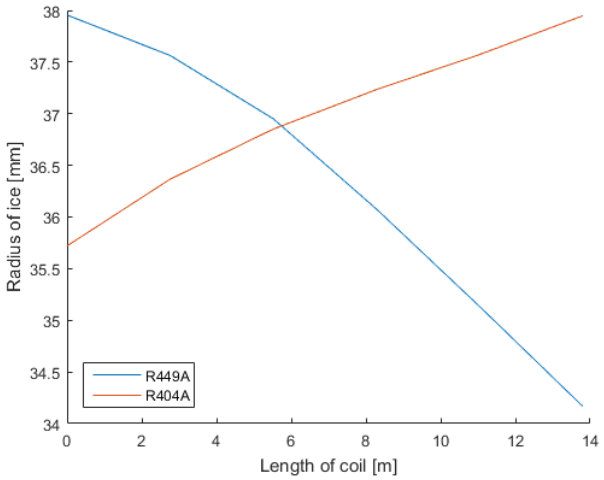

Figure 7: Ice radius distribution along the length.

The convection coefficient increases along the length because the boiling phenomenon is more profound when a larger vapour fraction of the refrigerant is present. As a result, the ice formation is expected to be enhanced along the length which is the case for R404A. However, the heat transfer is also dependent on the temperature difference between fluid and wall. The temperature glide of R449A is larger than the decrease in temperature difference between the refrigerant and the tube wall due to an increase in convection coefficient. The difference of the temperature glide between the two refrigerants is shown in Figure 8.
A drop of the evaporating temperature, visualized in Figure 8, is needed to ensure the continuation of the ice formation. Moreover, it also corresponds to a drop of the mass flow rate, which is a result of the constant volumetric flow rate of the compressor. Based on the storage capacity after the complete charging cycle, the switch from R404A to R449A would not be suggested. However, some additional benefits next to the decreased environmental impact are obtained. We can also determine the performance of the condensing unit by its coefficient of performance (COP):

$$COP = Q\ W^{-1} \qquad \text{Eq. (8)}$$

With Q the supplied cooling power and W the needed electric power input. The COP decreases with time as a result of the decreased evaporating temperature. The COP, visualized in Figure 9, is continuously larger (on average 10%) for R449A compared to R404A. As a result, the electricity consumption is lower.

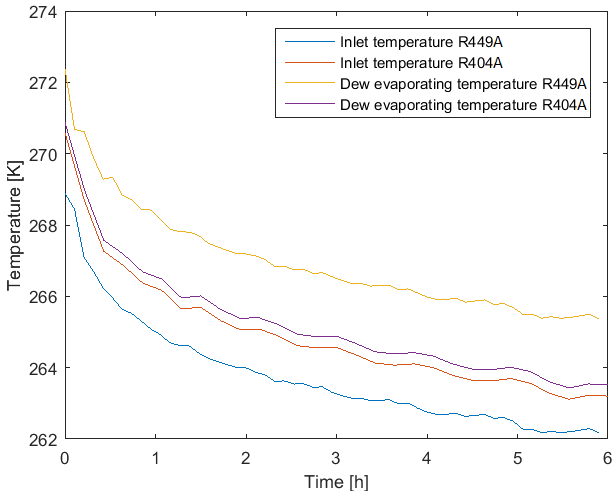

Figure 8: Inlet and dew evaporating temperatures during a complete charging cycle.

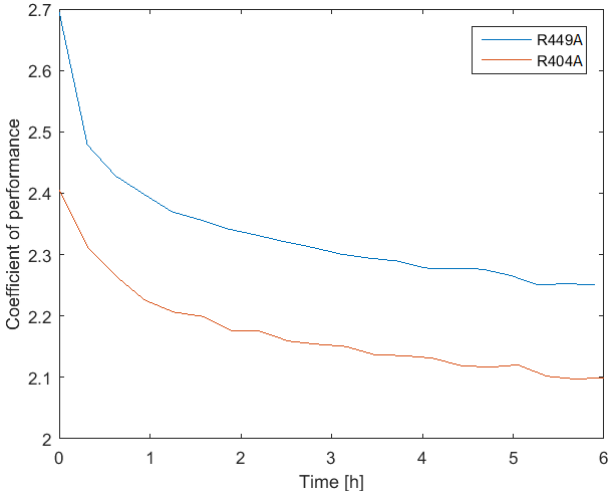

Figure 9: Coefficient of performance during a complete charging cycle.

4. CONCLUSIONS

A dynamic numerical model is developed in this work, based on the thermal resistance matrix method. It is capable to perform simulations on both the charging as well as the discharging process of an ice-on-coil external melt system and shows great similarity with data provided by the manufacturer and effectiveness curves from scientific literature. Numerical results indicate that an increased division in sections and layers converges to a defined limit value. The charging cycle is evaluated with the connection of the evaporator model to a condensing unit to study the effect of different refrigerants. To ensure the continuation of the ice formation with the increased ice thermal resistance, the inlet refrigerant temperature drops from 269.1 K to 263 K and as a result, the COP of the system decreases from 2.7 to 2.25. In the end a cooling capacity of 86.5 MJ is obtained (with five coils) and a total mass of ice of 255.08 kg. This is a deviation of 6.74 % in total ice capacity and 7.92 % in total mass compared to the theoretical maximum values. Furthermore, it was found that the switch of refrigerant from R404A to R449A is not only supported by its lower GWP and ODP value, but also by the increase in COP of around 10 %. However, numerical simulations showed a more uneven thickness distribution of R449A compared to R404A. As a result, the mass of ice is 1.823 kg lower and the corresponding ice capacity is 617 kJ lower per coil. To support the findings in this paper, an experimental setup is being constructed to validate the model thoroughly. With this validated model, it will be possible to design more efficient ice storage tanks.

NOMENCLATURE

b	input array (W)
c_p	heat capacity (J kg^{-1} K^{-1})
COP	coefficient of performance (-)
ext	external nodes
g	gravitational acceleration (m s^{-2})
GWP	global warming potential (-)
H	enthalpy (J kg^{-1})
H_{lat}	latent heat (J kg^{-1})
i,j,k	node indices
K	thermal conductance (W K^{-1})
m	mass (kg)
$\dot{m}_f$	fluid mass flow rate (kg s^{-1})
ODP	ozone depletion potential (-)
Q_{ice}	cooling capacity (W)
Q	heat (transfer) (W)
r	radius (m)
R	thermal resistance (K W^{-1})
Ra	Rayleigh number (-)
Re	Reynolds number (-)
T	temperature (K)
T_{melt}	melting temperature (K)
T_{wall}	outer temperature of the (ice) coil (K)
T_∞	average tank temperature (K)
v	fluid velocity (m s^{-1})
W	electric power input (W)
β	thermal expansion coefficient (K^{-1})
Δt	discretised time step (s)
ΔT	temperature difference (K)
ε	effectiveness (-)
μ	dynamic viscosity (Pa s)
ρ	density (kg m^{-3})

REFERENCES

Baltimore. 2019. Ice-on-coil external melt. Retrieved from https://www.baltimoreaircoil.eu/

Biosca-Taronger, J., Payá, J., López-Navarro, A., & Corberán, J., 2012. Ice formation modelling around the coils of an ice storage tank. Journal of Physics: Conference Series, 012133.

Candanedo, J., Dehkordi, V., & Stylianou, M., 2013. Model-based predictive control of an ice storage device in a building cooling system. Applied Energy 111, 1032-1045.

Cárdenas, B., & León, N., 2013. High temperature latent heat thermal energy storage: Phase change materials, design considerations and performance enhancement techniques. Renewable and Sustainable Energy Reviews 27, 724-737.

Goetzler, W., Guernsey, M., Young, J., Fuhrman, J., & Abdul-Aziz, O., 2016. The future of air conditioning for buildings. US Department of Energy, Office of Energy Efficiency and Renewable Energy Building Technologies Office report.

Ihm, P., Krarti, M., & Henze, G. P., 2004. Development of a thermal energy storage model for EnergyPlus. Energy and Buildings 36(8), 807-814.

Lee, A. H., & Jones, J. W., 1996. Modeling of an ice-on-coil thermal energy storage system. Energy Conversion and Management 37(10), 1493-1507.

Makhnatch, P., Mota-Babiloni, A., Rogstam, J., & Khodabandeh, R., 2017. Retrofit of lower GWP alternative R449A into an existing R404A indirect supermarket refrigeration system. International Journal of Refrigeration 76, 184-192.

Saito, A., 2002. Recent advances in research on cold thermal energy storage. International Journal of Refrigeration 25(2), 177-189.

Shah, M. M., 1976. A new correlation for heat transfer during boiling flow through pipes. Ashrae Trans. 82(2), 66-86.

Steinke, F., Wolfrum, P., & Hoffmann, C., 2013. Grid vs. storage in a 100% renewable Europe. Renewable Energy 50, 826-832.

Tecumseh. 2016. Guidelines for using R449A and R452A in new and existing commercial refrigeration.

Vetterli, J., & Benz, M., 2012. Cost-optimal design of an ice-storage cooling system using mixed-integer linear programming techniques under various electricity tariff schemes. Energy and Buildings 49, 226-234.

Yen, Y.-C., 1990. Natural convection heat transfer in water near its density maximum. U.S. Army Corps of Engineers, Cold Regions Research & Engineering Laboratory.